

Analytical model of optical properties of a metal nanorod

Cheng-ping Huang^{1*} and Xiao-gang Yin²

¹*Department of Physics, Nanjing Tech University, Nanjing 211816, China*

²*College of Physics, Nanjing University of Aeronautics and Astronautics, Nanjing
211106, China*

Abstract

It is well known that the optical properties of spherical metal particles can be described with the Rayleigh approximation or rigorous Mie theory. But for the small metallic nanorods, a theory well capturing the resonance and scattering features is still absent. In this paper, an analytical model is developed for the metallic nanorod, considering the non-uniformly distributed conduction current and surface charges. With the circuit parameters deduced from the kinetic and electromagnetic energy of the plasmonic system, a formula which agrees well with the simulations has been suggested for the resonance wavelength. Moreover, by introducing the radiative resistance to the circuit theory, the dipole moment, extinction spectrum, and the near-field enhancement of nanorod have been derived analytically and confirmed numerically. These results are valuable for understanding the plasmonic resonance and provide a guideline for designing the light scattering and absorption.

* Email: cphuang@njtech.edu.cn

I. Introduction

The photons and electrons, which are of different nature, may be coupled to generate the quasi-particles, i.e., the plasmon polaritons. For a flat metal surface, surface-plasmon polariton can be excited, propagating along the surface with subwavelength mode sizes. This surface mode plays an important role in the plasmonic waveguiding and light transmission through perforated metal films [1, 2]. On the other hand, the small metal particles, such as the nanospheres and nanorods etc., can support the localized surface-plasmon (LSP) resonance. The LSP resonance gives rise to strong field enhancement near the particle and enhanced scattering and absorption of incident light. The localized excitation has a number of potential applications, such as the plasmonic sensing [3], enhancement of Raman signal and harmonic generation [4, 5], photo-thermal therapy [6], and information storage [7], etc. Moreover, by using arrays of metal particles, various optical devices such as the plasmonic waveguides [8, 9], directional optical antennas [10], ultrathin metasurfaces [11-13], and plasmonic crystals [14-16] can be constructed.

Besides the experimental progress achieved so far, the theoretical studies are especially important for understanding the resonance effect and designing the particle-based devices. As is well known, for the spherical metal particles, the resonance effect can be uncovered with the Rayleigh approximation or Mie scattering theory [17]. Compared with the metal spheres, the plasmonic resonance of nanorods is strongly dependent on the aspect ratio [18], providing an efficient way to tune the resonance and thus attracting much more interest. But, up to now, a theory well capturing the resonance and scattering features of a metallic nanorod is still absent. By modeling the nanorod as elongated ellipsoid, empirical formulas with fitting parameters have been suggested to describe the resonance wavelength or scattering intensity [19-21]. However, the numerical simulations demonstrated that the plasmonic resonance features of the nanorod differ significantly from the ellipsoid [22]. Starting from the waveguide theory, Novotny has derived successfully the effective wavelength of an optical antenna consisting of a single metallic nanorod [23]. Nonetheless, the

complicated format makes it difficult to arrive at a direct and accurate expression for the resonance wavelength, especially when the rod radius is not too small. Moreover, the scattering and absorption features of the nanorod have not been addressed by the waveguide theory. In contrast, the circuit theory was employed in 2009 by the present authors and coauthors to study the plasmonic resonance of the nanorod [24]. But some excessive approximations, such as the homogeneous current distribution along the nanorod, the fitting parameter in the capacitance [25] etc., have been used. More importantly, the width and magnitude of the extinction spectrum predicted by the theory do not agree with the numerical simulations.

In this paper, an analytical model has been developed for the metallic nanorod, which well reproduces the plasmonic resonance wavelength, the scattering/absorption /extinction spectrum, and the near-field enhancement. The model is based on the circuit theory but the theoretical analysis highlights the energy aspect of the plasmonic system. In the theoretical treatment, non-uniform distributions of the conduction currents and surface charges have been considered and the radiative resistance of the nanorod has been introduced. These contribute to the good agreement between the theory and simulations and are helpful for uncovering the underlying physics. The paper is organized as follows. In Sec. II, the circuit parameters of the nanorod have been derived, considering the energy stored in the plasmonic system. An analytical formula for the resonance wavelength of the nanorod is obtained in Sec. III. The dependence of resonance wavelength on the geometrical and material parameters has been suggested and compared with the simulations. In Sec. IV, the dipole moment of the nanorod is deduced with the circuit equation, where the radiative resistance has been determined and employed. The resonance broadening associated with both the radiative resistance and Faraday inductance is revealed. The scattering, absorption, and extinction cross sections are given in Sec. V. The evolution of extinction spectrum with the parameters is discussed and a systematic comparison between the theory and simulations is made as well. The Sec. VI calculates the enhancement ratios of the electric and magnetic field in the near zone of nanorod. And a short summary is presented in Sec. VII.

II. Circuit parameters

The metallic nanorod considered here is schematically shown in Fig. 1, which has two hemispherical ends [18, 19]. The radius of nanorod is r_0 and the total length is l ($l \gg r_0$). The nanorod is embedded in a dielectric medium with the permittivity of ϵ_d . The incident light propagates with the electric field along the axis of nanorod, exciting the longitudinal plasmonic resonance. We suppose that the radius of the nanorod is much larger than the Fermi wavelength but smaller than the skin depth of metal [$\lambda_F (\sim 0.5 \text{ nm}) \ll r_0 \leq \delta (\sim 20 \text{ nm})$], thus the quantum effect can be neglected and the fields in the cross section of the nanorod can be taken to be homogeneous.

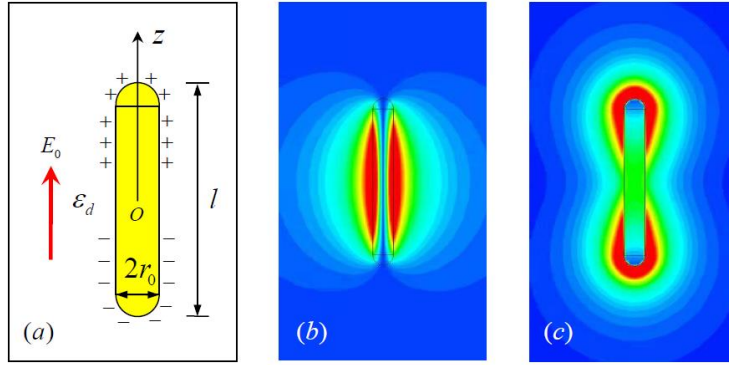


Fig. 1 (a) Schematic view of single metallic nanorod, which is embedded in a dielectric medium and excited by a longitudinal light electric field. (b, c) Amplitude distributions of magnetic field (b) and electric field (c) at the plasmonic resonance.

In the optical frequency range, the free electrons in the metallic nanorod play a dominant role and the effect of bounded electrons can be ignored. When the sizes of the metal particles are much smaller than the wavelength, the quasi-static approach may be applicable and the circuit parameters such as the inductance and capacitance can be used [26]. Under the action of longitudinal light electric field, the oscillating conduction current can be induced in the nanorod. Correspondingly, positive and negative charges are accumulated on the nanorod surface, i.e., the side and ends of the nanorod. Accompanying the oscillation of current and surface charges, there are kinetic energy of moving free electrons, electric-field energy of surface charges, and

magnetic-field energy of conduction current stored in the plasmonic system. Consequently, by calculating the kinetic and electromagnetic energy analytically, the circuit parameters of the nanorod may be determined [27].

The numerical simulation showed that, for the fundamental plasmonic resonance, the conduction current along the nanorod is not uniformly distributed [27]. Instead, a standing-wave-like pattern is present for the conduction current, which is maximal at the center of nanorod and zero near the two ends. The complex conduction current density can be approximated by [23]

$$J(z) = J_0 \cos(\pi z / l) e^{-i\omega t}, \quad (1)$$

where $z \in [-l/2, l/2]$ and J_0 is the magnitude of current density at the center of nanorod. Correspondingly, the surface density of free charges can be expressed as

$$\rho(z) = i\rho_0 \sin(\pi z / l) e^{-i\omega t}, \quad (2)$$

where ρ_0 is the magnitude of surface charge density near the two ends. By using the law of charge conservation $SdJ = -d(\rho 2\pi r_0 dz) / dt$ in the volume element $dV = Sdz$ ($S = \pi r_0^2$ is the cross-sectional area of the nanorod), the relationship between the magnitude of surface charges and conduction current can be determined as

$$J_0 = (2l / \pi r_0) \rho_0 \omega. \quad (3)$$

With the Eq. (2), some useful results can be deduced. One result is that the total surface charges accumulated on the upper half part of the nanorod are

$$\begin{aligned} Q &= \rho(0.5l) 2\pi r_0^2 + \int_0^{0.5l-r_0} \rho(z) 2\pi r_0 dz \\ &= iQ_0 e^{-i\omega t}. \end{aligned} \quad (4)$$

Here, the first and second term on the right-hand side of Eq. (4) represents the charges accumulated on the end and side of the nanorod, respectively; $Q_0 = 2\rho_0 r_0 l$ is the magnitude of oscillating free charges on half a nanorod. We can deduce that the fraction of charges distributed on the semispherical end is $R = \pi r_0 / l$. For a nanorod with an aspect ratio of $\kappa = l / 2r_0 = 5$, for example, about 31% surface charges

distribute on the end and 69% charges on the side of nanorod. Another result is the dipole moment of the nanorod. For convenience, we treat all the positive (or negative) free charges as a point charge Q (or $-Q$) with the position locating at the center of charges z_0 (or $-z_0$). With the Eqs. (2) and (4), we obtain

$$z_0 = \int z dq / Q = l / \pi. \quad (5)$$

Then, the distance between the centers of positive and negative charges is $\Delta z = 2l / \pi$. Correspondingly, the dipole moment of the nanorod is

$$p = (2 / \pi) Ql. \quad (6)$$

Based on the above results, the kinetic and electromagnetic energy of free charges or currents have been calculated and the circuit parameters have been derived. For the kinetic energy of free electrons, by setting $U_K = (1/2)L_K I_m^2$ (where $I_m = J_0 S \cos \omega t$ is the real and spatially maximal current at the center of nanorod), the kinetic inductance is obtained as (see Appendix A):

$$L_K = \frac{\mu_0 l}{2\pi} \left(\frac{\delta}{r_0}\right)^2. \quad (7)$$

Here, δ is the skin depth of the metal. Thus, the kinetic inductance is dominated by the length and radius of the nanorod. Especially, it will play a critical role when the rod radius is comparable with or smaller than the skin depth of the metal. Due to the decrease of electron velocity near the ends of nanorod, the kinetic inductance is significantly reduced, which is just half the result of the uniform-current case [24].

The conduction current will excite an enhanced magnetic field within and outside the nanorod, as shown in Fig. 1(b). By calculating the total magnetic-field energy approximately and setting $U_M = (1/2)L_F I_m^2$, the Faraday inductance of the nanorod can be obtained as (see Appendix B):

$$L_F = \frac{\mu_0 l}{4\pi} \left(\ln 2\kappa + \frac{1}{4}\right). \quad (8)$$

Thus, the Faraday inductance is governed by the length l and aspect ratio κ of the nanorod. Similarly, compared with the case of uniform current distribution, the Faraday inductance is also reduced.

Figure 1(c) shows that the accumulation of free charges on the surface of the nanorod can induce an enhanced electric field in the surrounding space. The electric energy includes not only the electric-field energy of the isolated positive and negative charges but also the interacting electric potential energy of them. By setting $U_E = Q_m^2 / 2C$ (where $Q_m = Q_0 \sin \omega t$), the capacitance of nanorod is determined as (see Appendix C):

$$C = \frac{4\varepsilon_0\varepsilon_d\kappa l}{(2\pi - \kappa) + \pi(\kappa - 2)\ln \kappa}. \quad (9)$$

Thus, the capacitance of nanorod is dependent on the rod length l , aspect ratio κ , and the permittivity ε_d of the surrounding medium.

III. Resonance wavelength

3.1 Analytical formula of resonance wavelength

At the free resonance (the Ohmic loss and radiation loss of the nanorod are neglected), the total kinetic and electromagnetic energy of the system will be conserved. That is

$$\frac{1}{2}L_K I_m^2 + \frac{1}{2}L_F I_m^2 + \frac{Q_m^2}{2C} = \text{const}. \quad (10)$$

By calculating the derivative of the total energy versus time and noticing that $I_m = dQ_m / dt$, one obtains

$$\frac{d^2}{dt^2} Q_m + \frac{1}{(L_K + L_F)C} Q_m = 0. \quad (11)$$

Thus the plasmonic resonance frequency of the nanorod is

$$\omega_0 = \frac{1}{\sqrt{(L_K + L_F)C}}. \quad (12)$$

By substituting the kinetic inductance, Faraday inductance, and capacitance into the Eq. (12), the vacuum resonance wavelength can be derived as

$$\lambda_0 = 4\kappa n_d \sqrt{\frac{2\delta^2 + (\ln 2\kappa + 1/4)r_0^2}{(2/\kappa - 1/\pi) + (1 - 2/\kappa)\ln \kappa}}. \quad (13)$$

Here, n_d is the refractive index of the surrounding medium. Thus, the resonance wavelength is determined by the material properties (the surrounding medium index n_d and the metal skin depth δ) and the geometrical parameters (the aspect ratio κ and the rod radius r_0) of the nanorod. Especially, the resonance wavelength is proportional to the refractive index n_d , which provides an efficient tuning method.

3.2 Dependence of resonance wavelength on the parameters

Based on the Eq. (13), the dependence of resonance wavelength on the aspect ratio, rod radius, and medium index has been calculated and the results are plotted with the lines in Figs. 2(a), 2(b) and 2(c), respectively. Moreover, to verify the validity of theory, numerical simulations based on the finite-difference time-domain (FDTD) method have been carried out [28]. In the simulation, the dispersion of metal is described with the Drude model $\epsilon_m = 1 - \omega_p^2 / \omega(\omega + i\gamma)$, where the plasma frequency is $\omega_p = 1.37 \times 10^{16}$ rad/s (corresponding to a skin depth $\delta = 22$ nm) and the collision frequency of free electrons is $\gamma = 5 \times 10^{13}$ Hz. The mesh size in the nanorod is set as 0.2-1.0 nm, depending on the sizes of the nanorod (a larger mesh size is used for the larger nanorod). With the numerical simulations, the extinction spectrum of the nanorod can be obtained (as shown in Sec. V) and the resonance wavelength extracted from the extinction spectra is mapped in Fig. 2 by the circles.

The resonance wavelength as a function of aspect ratio is shown in Fig. 2(a), where the nanorod is in vacuum and the rod radius is fixed as 10 nm. The resonance wavelength increases almost linearly with the aspect ratio κ . When κ varies from 5 to 15 (or $l=100$ -300 nm), the resonance wavelength predicted by the Eq. (13) increases from 683 to 1490 nm, approaching the simulation values from 663 to 1544 nm (the largest deviation is 3.5% for $\kappa=15$). In Fig. 2(b), the resonance wavelength as a function of rod radius is shown, where the nanorod with a constant aspect ratio $\kappa=8$ is put in vacuum. One can see that the resonance wavelength grows obviously and nonlinearly with the rod radius. When r_0 varies from 5 to 20 nm, the resonance wavelength increases from 846 to 1221 nm analytically and from 879 to 1168 nm

numerically (the maximal deviation is 4.5% for $r_0=20$ nm). Thus the aspect ratio alone cannot determine the plasmonic resonance wavelength [22]. This is associated with the Faraday inductance [according to the Eq. (12), the resonance wavelength will be independent of the rod radius if L_F is neglected]. In addition, we fix the sizes of nanorod ($\kappa=8$ and $r_0=10$ nm) and change the refractive index of the surrounding medium. The resonance wavelength as a function of medium index is present in Fig. 2(c). When n_d changes from 1.0 to 2.0, the analytical resonance wavelength increases linearly from 934 to 1868 nm, which is in good accordance with the simulation results (from 942 to 1894 nm; the largest deviation between them is 1.8%). The strong dependence of resonance wavelength on the surrounding medium index is valuable for the sensing applications [3].

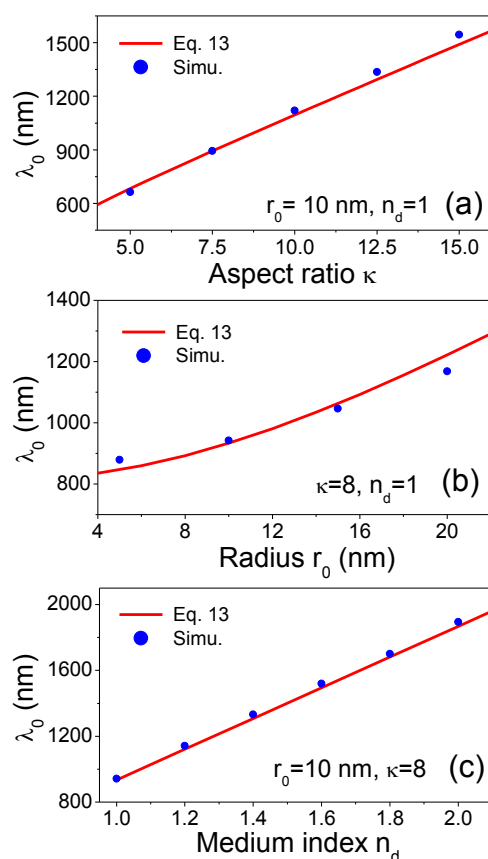


Fig. 2 Resonance wavelength of the nanorod as a function of (a) aspect ratio ($r_0=10$ nm, $n_d=1$), (b) the rod radius ($\kappa=8$, $n_d=1$), and (c) the medium index ($\kappa=8$, $r_0=10$ nm), respectively. Here, the lines represent the analytical results and the circles the simulation results.

IV. Dipole moment

The plasmonic resonance of the nanorod is excited by the incident light. Thus the conduction current and surface charges will be strongly dependent on the light electric field E_0 . In the subwavelength region ($2r_0 \ll l \ll \lambda$), such a relationship may be bridged approximately with the circuit theory. Nonetheless, the non-uniform current distribution along the rod axis hinders the direct application of the circuit equation. To address this question, an equivalent method will be used in the following. Another key point is that the radiative resistance, which is not present in the conventional circuit theory but plays an important role in the nano-optics, will be counted here.

Considering the circuit parameters introduced above, an effective induced electromotive force $-L_F dI_c / dt$ (where $I_c = J_0 S e^{-i\omega t}$ is the complex current at the center of nanorod) and an effective electric potential difference $-Q/C$ will be exerted on the nanorod. The equivalent circuit equation, which determines the central current I_c of the nanorod, may be written as

$$\xi_{eff} - L_F \frac{dI_c}{dt} - \frac{Q}{C} = I_c (R_{rod} + R_{rad}), \quad (14)$$

where ξ_{eff} represents the effective electromotive force contributed by the light electric field, R_{rod} is the effective electric resistance (or impedance) of the nanorod, and R_{rad} is the effective resistance resulting from the radiation loss. The radiation of light will consume the energy of oscillating free electrons, thus an additional damping force is applied to the electrons, leading to an effective radiative resistance. Equation (14) can also be derived with the energy conservation.

The effective electromotive force ξ_{eff} will transfer the energy from the incident light to the nanorod with an average power $P_{in} = (1/2) \text{Re}(I_c^* \xi_{eff})$ (here * represents the complex conjugation). The input power can be obtained by performing the integral over the whole nanorod:

$$P_{in} \approx \frac{1}{2} \text{Re} \int_{-l/2}^{l/2} [J(z)S]^* E_0 dz = \frac{1}{2} \text{Re}(I_c^* E_0 \frac{2l}{\pi}). \quad (15)$$

Thus, the effective electromotive force driven by the light field reads

$$\xi_{eff} = E_0 \Delta z = (2/\pi) E_0 l. \quad (16)$$

Here, $\Delta z = 2l/\pi$ is the effective length, which is also the central distance of positive and negative charges $\pm Q$.

To calculate the effective resistance R_{rod} , one notes that the power of effective R_{rod} should be equal to that of the real nanorod. That means

$$\frac{1}{2} |I_c|^2 R_{rod} = \frac{1}{2} \int |J(z)S|^2 dR, \quad (17)$$

where $dR = dz/\sigma S$. By using the Eq. (1) and $\sigma = \sigma_0/(1-i\omega\tau)$, the R_{rod} can be derived as

$$R_{rod} = \frac{1}{\sigma} \frac{l}{2S} = R_{Ohm} - i\omega L_K. \quad (18)$$

Here, $R_{Ohm} = l/2\sigma_0 S = \gamma L_K$ is the dc Ohmic resistance, $L_K = \mu_0 l/2k_p^2 S$ (where $k_p = \omega_p/c = 1/\delta$) is exactly the kinetic inductance of the nanorod. Thus, in the optical frequency range, the nanorod behaves like the series connection of a pure dc resistance R_{Ohm} and an inductor L_K .

The effective radiative resistance R_{rad} can be determined with the radiation energy. That is, the power consumed in R_{rad} equals the radiation power of the real nanorod. According to the Eq. (6), the dipole moment of the nanorod is $p = (2/\pi)Ql$ and thus the radiation power is

$$P_{rad} = \frac{1}{2} |I_c|^2 R_{rad} = \frac{\mu_0 n_d}{12\pi c} \omega^4 |p|^2. \quad (19)$$

The central current and surface charges satisfy the relationship $I_c = dQ/dt = -i\omega Q$.

Consequently, the effective radiative resistance is expressed as

$$R_{rad} = \frac{2\mu_0 n_d}{3\pi^3 c} \omega^2 l^2 = \frac{8}{3\pi} \left(\frac{n_d l}{\lambda}\right)^2 Z, \quad (20)$$

where $Z = \sqrt{\mu_0/\epsilon_0 \epsilon_d}$ is the impedance of the surrounding medium.

By substituting ξ_{eff} , R_{rod} and R_{rad} into the Eq. (14), the relationship between the central oscillating current I_c and light electric field E_0 can be established. Accordingly, the dipole moment induced in the nanorod is derived as

$$p = \frac{\varepsilon_0 A}{\omega_0^2 - \omega^2 - i\eta\omega} E_0, \quad (21)$$

where

$$A = \frac{(2l/\pi)^2}{\varepsilon_0(L_K + L_F)}, \quad (22)$$

$$\eta = \frac{R_{Ohm} + R_{rad}}{L_K + L_F}.$$

Hence, the induced dipole moment is proportional to the external light electric field E_0 and resonant at the frequency ω_0 with a bandwidth η (the quality factor is $Q = \omega_0/\eta$). Especially, the resonance bandwidth η is proportional to the total resistance ($R_{Ohm} + R_{rad}$) and inversely proportional to the total inductance ($L_K + L_F$). If both the radiative resistance and Faraday inductance are ignored, η will be degenerated exactly to γ , i.e., the collision frequency of the free electrons. However, the presence of the radiative resistance and Faraday inductance will modify (broaden) the width of resonance. This point will be confirmed by the simulations.

V. Extinction spectrum

5.1 Scattering, absorption, and extinction spectra

The plasmonic resonance of the nanorod is accompanied by a strong scattering and absorption of light. To calculate the scattering, absorption, and extinction cross sections, we define the polarizability of nanorod as $\chi = p/\varepsilon_0 E_0$. By normalizing the radiation power P_{rad} of the nanorod with the intensity of incident light $I_l = \varepsilon_0 c n_d E_0^2 / 2$, the scattering cross section can be expressed as $C_{sca} = k_0^4 |\chi|^2 / 6\pi$, where k_0 is the wavevector in the free space. Moreover, according to the Eq. (15),

the power consumed in the nanorod can be rewritten as $P_{in} = \text{Re}(p E_0^*)/2$. Actually, this power includes both the Ohmic and radiation loss (as the radiation resistance has been taken into account in the circuit equation). Thus, by normalizing P_{in} with I_l , the extinction cross section is obtained as $C_{ext} = (k_0/n_d)\text{Im}\chi$. The difference between C_{ext} and C_{sca} gives rise to the absorption cross section: $C_{abs} = C_{ext} - C_{sca}$ (which can also be obtained with $C_{abs} = |I_c|^2 R_{Ohm} / 2I_l$).

With the polarizability χ deduced from the Eq. (21), one obtains

$$\begin{aligned} C_{sca} &= \frac{A^2}{6\pi c^4} \frac{\omega^4}{(\omega_0^2 - \omega^2)^2 + \eta^2 \omega^2}, \\ C_{ext} &= \frac{A\eta}{n_d c} \frac{\omega^2}{(\omega_0^2 - \omega^2)^2 + \eta^2 \omega^2}. \end{aligned} \quad (23)$$

One can also obtain with the Eqs. (23) that $C_{sca} / C_{ext} = R_{rad} / (R_{Ohm} + R_{rad})$. At the plasmonic resonance of the nanorod, the maximum of the scattering, absorption, and extinction cross sections can be derived, respectively, as

$$\begin{aligned} C_{sca}^m &= \left(\frac{2l}{\pi}\right)^2 \frac{ZR_{rad}}{(R_{Ohm} + R_{rad})^2}, \\ C_{abs}^m &= \left(\frac{2l}{\pi}\right)^2 \frac{ZR_{Ohm}}{(R_{Ohm} + R_{rad})^2}, \\ C_{ext}^m &= \left(\frac{2l}{\pi}\right)^2 \frac{Z}{R_{Ohm} + R_{rad}}. \end{aligned} \quad (24)$$

Then, the ratio $Z / (R_{Ohm} + R_{rad})$ measures the maximal ability of energy transfer from the incident light to the nanorod. Note that the spectral width η is proportional to the total resistance, i.e., $\eta \propto R_{Ohm} + R_{rad}$ [see Eqs. (22)]. Thus, the larger the total resistance, the lower the peak of extinction spectrum and the wider the spectral width. In addition, Eqs. (24) show that $R_{rad} / (R_{Ohm} + R_{rad})$ governs the radiation of energy from the nanorod to the surrounding space and $R_{Ohm} / (R_{Ohm} + R_{rad})$ dominates the fraction of energy dissipated in the Ohmic loss. The results provide a useful guideline for the optimization of light scattering or absorption of the metallic nanorods.

5.2 Dependence of extinction spectrum on the parameters

To grasp the detailed characteristics of the scattering, absorption, and extinction spectra, we take the nanorod with a length $l=160$ nm and radius $r_0=10$ nm (in vacuum) as an example. Figure 3(a) presents the calculation results by using the Eqs. (23), with the resonance frequency ω_0 determined by the Eq. (13). One can see that there is a prominent peak, locating at the resonance wavelength $\lambda_0=934$ nm, in each spectrum. Thus, the plasmonic resonance of the nanorod is accompanied by the strong scattering, absorption, and extinction of light. The full-width at half-maximum (FWHM) of the peak is $\Delta\lambda=39$ nm, thus corresponding to a Q factor of 23.9. The frequency range of the FWHM can be determined by $\Delta\omega=2\pi c(\Delta\lambda/\lambda_0^2)$ or $\eta=(R_{Ohm}+R_{rad})/(L_K+L_F)$. Using the known parameters, we have $L_K=0.155$ pH, $L_F=0.048$ pH, $R_{Ohm}=\gamma L_K=7.74\ \Omega$, and $R_{rad}=9.38\ \Omega$. Hence, the spectral width is calculated as $\Delta\omega=\eta=8.44\times 10^{13}$ Hz, which is obviously larger than the employed electron collision frequency $\gamma=5\times 10^{13}$ Hz. In addition, the maximal scattering, absorption, and extinction cross sections can be obtained from the spectra [or with the Eqs. (24)] as 0.125, 0.103, and 0.228 μm^2 , respectively. The maximal extinction efficiency $C_{ext}^m/2r_0l$, i.e., the maximal extinction cross section normalized by the projection area of the nanorod (on the plane perpendicular to the light propagation direction), attains a large value of 71.

As a comparison, Fig. 3(b) presents the simulated scattering, absorption, and extinction spectra. The peaks of the spectra locate at the wavelength $\lambda_0=942$ nm with a FWHM of $\Delta\lambda=44$ nm and a Q factor of 21.4. The frequency range of FWHM is $\Delta\omega=9.34\times 10^{13}$ Hz, which is also larger than γ and close to the analytical value $\eta=8.44\times 10^{13}$ Hz, thus confirming the role of the radiative resistance and Faraday inductance. Furthermore, the maximal scattering, absorption, and extinction cross sections given by the simulation are 0.124, 0.105, and 0.229 μm^2 , respectively, which

agree well with the analytical results (0.125, 0.103, and 0.228 μm^2).

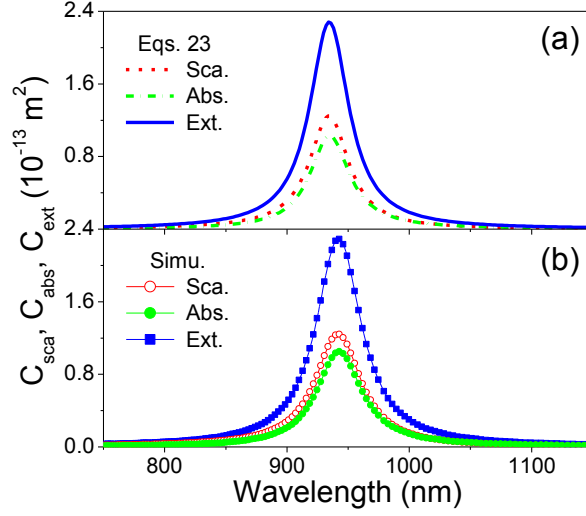


Fig. 3 Scattering, absorption, and extinction spectra of the nanorod obtained with the analytical formulas (a) and numerical simulations (b). Here, the rod length is $l=160$ nm, the radius is $r_0=10$ nm, and the surrounding medium is vacuum.

By varying the structural and material parameters, we investigated the evolution of extinction spectrum of the nanorod. The results are shown in Fig. 4, where the left column (a, c, e) represents the analytical results and the right column (b, d, f) the numerical simulations. Figures 4(a, b) show the variation of extinction spectrum with the increase of the aspect ratio κ , where $r_0=10$ nm and $n_d=1$. According to the analytical results, when κ varies from 5 to 7.5, 10, 12.5, and 15, the maximal extinction cross section C_{ext}^m increases almost linearly from 0.131 to 0.211, 0.300, 0.397, and 0.500 μm^2 (along with the redshift of the resonance peak). The results are in agreement with the simulations, where C_{ext}^m grows from 0.119 to 0.209, 0.306, 0.411, and 0.519 μm^2 . Equation (24) suggests that $C_{ext}^m \propto l^2 Z / (R_{Ohm} + R_{rad})$, where $Z \propto 1/n_d$, $R_{Ohm} \propto l/r_0^2$, and $R_{rad} \propto (n_d l / \lambda_0)^2 Z$. In present case, the resonance wavelength is nearly proportional to the aspect ratio or rod length [see Fig. 2(a)], thus R_{rad} is almost a constant at the resonance. Consequently, $C_{ext}^m \propto l^2 / (l + c_1)$ (where c_1 is a constant), which varies almost linearly with l (or κ) when l is larger enough.

Moreover, the extinction energy is separated into two parts, one is the scattering with the fraction $R_{rad}/(R_{Ohm} + R_{rad}) \propto 1/(l + c_1)$ and the other is the absorption with the fraction $R_{Ohm}/(R_{Ohm} + R_{rad}) \propto l/(l + c_1)$. The latter acquires a further enhancement, indicating that the longer nanorod (with the fixed radius) is more helpful for the light absorption and the photo-thermal effect.

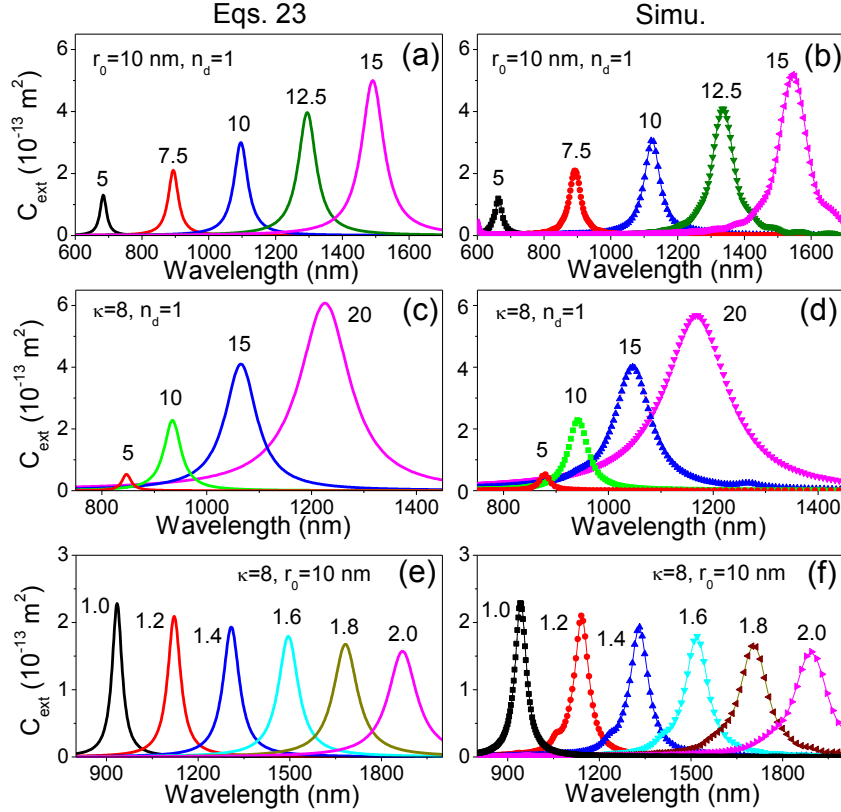


Fig. 4 Extinction spectra of the nanorod: (a, b) $r_0=10$ nm, $n_d=1$, the aspect ratio is set as $\kappa=5, 7.5, 10, 12.5$, and 15 , respectively; (c, d) $\kappa=8$, $n_d=1$, the rod radius is set as $r_0=5, 10, 15$, and 20 nm, respectively; (e, f) $\kappa=8$, $r_0=10$ nm, the refractive index of the surrounding medium is set, respectively, as $n_d=1.0, 1.2, 1.4, 1.6, 1.8$, and 2.0 . The left column (a, c, e) represents the analytical results obtained with the Eqs. (23) and the right one (b, d, f) the simulation results.

Figures 4(c, d) exhibit the extinction spectra for different rod radius, where $n_d=1$ and the aspect ratio is fixed as $\kappa=8$. When the radius varies from 5 to 10, 15, and 20 nm, analytically C_{ext}^m increases from 0.053 to 0.228, 0.411, and 0.608 μm^2 ; and

numerically, C_{ext}^m grows from 0.053 to 0.229, 0.401, and 0.569 μm^2 . The larger deviation of C_{ext}^m ($\sim 7\%$) for $r_0=20$ nm is mainly caused by the deviation of resonance wavelength ($\sim 4.5\%$). If we use the numerical resonance wavelength (1168 nm) rather than the analytical value (1221 nm) to determine the radiative resistance R_{rad} , Eq. (24) will give $C_{ext}^m = 0.561 \mu\text{m}^2$, which is much closer to the simulated value 0.569 μm^2 . When the aspect ratio is fixed, we obtain $C_{ext}^m \propto 1/(V^{-1} + c_2\lambda_0^{-2})$, where V is the volume of nanorod and c_2 is a constant. Thus, a larger nanorod with a longer resonance wavelength is beneficial for the extinction of light. Moreover, the fraction of scattering light is proportional to $1/(c_2 + \lambda_0^2/V)$, which can be further enhanced. On the contrary, a thinner nanorod with the fixed aspect ratio will own a larger fraction of light absorption.

Additionally, when the rod sizes are fixed and the refractive index of the surrounding medium is increased, C_{ext}^m will be reduced along with the redshift of the resonance peak. The analytical results in Fig. 4(e) show that, when n_d changes from 1.0 to 2.0 with an interval of 0.2 ($\kappa=8$, $r_0=10$ nm), C_{ext}^m decreases gradually from 0.228 to 0.209, 0.193, 0.180, 0.168, and 0.157 μm^2 . Again, the results are in good accordance with the simulation results in Fig. 4(f), where C_{ext}^m reduces from 0.229 to 0.210, 0.193, 0.180, 0.165, and 0.157 μm^2 . In this case, the radiative resistance $R_{rad} \propto (n_d l / \lambda_0)^2 Z$ will only vary with the impedance Z of the surrounding medium, as the resonance wavelength is proportional to the medium index n_d [see the Eq. (13) or Fig. 2(c)]. Hence, $C_{ext}^m \propto 1/(n_d + c_3)$ (c_3 is a constant), which decreases with the increase of medium index. The fraction of light scattering is also proportional to $1/(n_d + c_3)$ and degenerates simultaneously.

VI. Field enhancement

The plasmonic resonance of the nanorod can induce a strong field enhancement near the metal surface [29]. On the surface of the two semispherical ends, surface charges are accumulated with a maximal density, thus leading to a maximal electric field $E_{end} = \rho_0 / \varepsilon_0 \varepsilon_d$. With the use of Eqs. (4) and (21), we obtain the frequency-dependent electric-field enhancement ratio as

$$\left| \frac{E_{end}}{E_0} \right| = \frac{\pi A}{4\varepsilon_d r_0 l^2} \frac{1}{\sqrt{(\omega_0^2 - \omega^2)^2 + \eta^2 \omega^2}}. \quad (25)$$

At the resonance, the maximal enhancement ratio becomes

$$\left| \frac{E_{end}}{E_0} \right|_{\max} = \frac{\lambda_0}{2\pi^2 n_d r_0} \frac{Z}{R_{Ohm} + R_{rad}}. \quad (26)$$

On the other hand, the oscillating current induces a strong magnetic field, which is maximal at the waist ($r = r_0$, $z = 0$) of the nanorod: $H_{mid} = J_0 r_0 / 2$. The magnetic-field enhancement ratio can be derived as

$$\left| \frac{H_{mid}}{H_0} \right| = \frac{A}{4r_0 \ln_d c} \frac{\omega}{\sqrt{(\omega_0^2 - \omega^2)^2 + \eta^2 \omega^2}}. \quad (27)$$

The maximal enhancement ratio at the resonance is

$$\left| \frac{H_{mid}}{H_0} \right|_{\max} = \frac{2\kappa}{\pi^2} \frac{Z}{R_{Ohm} + R_{rad}}. \quad (28)$$

One can see that the maximal electric- and magnetic-field enhancement ratios are correlated with the peak value of extinction cross section. The larger the extinction cross section, the larger the energy stored in the system and magnitude of surface charges and conduction current, thus the larger the electric and magnetic field.

We take the nanorod with a length $l=160$ nm and radius $r_0=10$ nm (in vacuum) as an example. Figure 5(a) presents the analytical enhancement ratio of electric field (at the end of nanorod; the solid line) and magnetic field (at the waist of nanorod; the dash line) as a function of wavelength. The calculation shows that, near the wavelength 934 nm, the electric and magnetic fields are enhanced by 104.1 and 35.6 times, respectively. Also, by setting the probes at the end or waist of the nanorod, the enhancement ratios of electric field (the solid circles) and magnetic field (the open

circles) have been simulated and plotted in Fig. 5(b). Near the wavelength 942 nm, the simulated electric field is enhanced by 85.4 times and magnetic field enhanced by 32.0 times, which are smaller but close to the analytical values [we found in the simulations that, by decreasing the mesh sizes of the nanorod, the numerical results of field enhancement will approach the analytical values gradually (here the mesh size was set as 0.2 nm)]. The small mode volume and strong near-field enhancement are important for boosting the light-matter interactions [30].

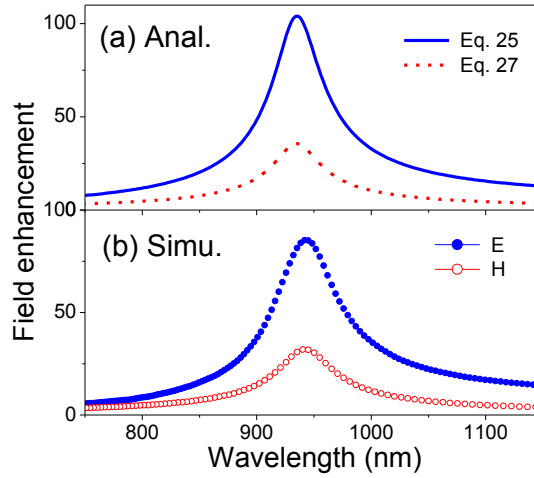


Fig. 5 Enhancement of electric field (at the end of nanorod) and magnetic field (at the waist of the nanorod) as a function of wavelength: (a) Analytical and (b) simulated results. Here, the rod length is $l=160$ nm, the radius is $r_0=10$ nm, and the surrounding medium is vacuum.

VII. Conclusions

In summary, an analytical model has been developed to study the optical properties of a metallic nanorod. In this model, non-uniform distributions of conduction current and surface charges in/on the nanorod were considered. With the calculation of kinetic and electromagnetic energy of the system, the circuit parameters of the nanorod have been determined. The plasmonic resonance wavelength predicted by theory agrees well with the simulations. Moreover, by introducing the radiative resistance to the circuit theory, the dipole moment, extinction spectrum, and near-field enhancement of the nanorod have been deduced analytically and confirmed numerically. These results

are valuable for several reasons. Firstly, our results present a fast way to calculate the plasmonic resonance of the nanorod, such as the resonance wavelength, scattering, absorption, and extinction spectra, etc. In contrast, the pure numerical simulations rely heavily on the computer resources and are highly time consuming. Secondly, the results are useful for understanding the resonance effects, such as the spectral broadening of plasmonic resonance, the dependence of resonance wavelength and extinction spectrum on the geometrical or medium parameters, etc. Finally, the analytical formulas may provide a guideline for designing the nanorod sizes, thus enhancing/suppressing the light scattering at certain wavelength or maximizing the light absorption in the photo-thermal effect.

ACKNOWLEDGMENTS

This work was supported by the National Natural Science Foundation of China (Grant No. 12174193).

Appendix A

Compared with the electric- or magnetic-field energy of a system, the kinetic energy of free electrons in the metal can be neglected in the low-frequency band. But in the optical range, the situation changes significantly: the latter contributes a lot to the energy of system. The kinetic inductance originates from the kinetic energy or inertia of free electrons. For the nanorod studied here, the velocity of free electrons, $v = J(z)/(-ne)$, will vary in space. With the Eq. (1), the kinetic energy of all moving electrons, $U_K = \sum_i (1/2)mv_i^2$, can be calculated as

$$\begin{aligned} U_K &\approx \int_{-l/2}^{l/2} \frac{1}{2} m \left[\frac{J_0 \cos(\pi z/l) \cos \omega t}{-ne} \right]^2 n S dz \\ &= \frac{1}{4} \frac{\mu_0 l}{k_p^2 S} I_0^2 \cos^2 \omega t. \end{aligned} \quad (\text{A1})$$

Here, $I_0 = J_0 S$ and $k_p = \omega_p / c = 1/\delta$ (δ is the skin depth of the metal). In the calculation, the cross-sectional area of the nanorod is treated as a constant throughout the rod length l , which will overestimate the kinetic energy of electrons. But this effect is very weak, as the conduction current and electron velocity approach zero near the two ends of the nanorod.

For the spatially uniform current distribution I , the kinetic inductance L_K can be simply introduced by $U_K = (1/2)L_K I^2$. Here, as the conduction current is varying along the rod axis, the real current I is defined as the spatial maximum at the center of nanorod, i.e., $I_m = I_0 \cos \omega t$. Consequently, the kinetic inductance is written as

$$L_K = \frac{\mu_0 l}{2k_p^2 S} = \frac{\mu_0 l}{2\pi} \left(\frac{\delta}{r_0}\right)^2. \quad (\text{A2})$$

Appendix B

Compared with the kinetic inductance that is linked to the kinetic energy of free electrons, the Faraday inductance is correlated with the magnetic-field energy outside and inside the nanorod. According to the magnetic loop theorem, the magnetic field excited by the conduction current is $H_{in} = Jr/2$ in the nanorod and $H_{out} \approx JS/2\pi r$

outside but near the nanorod. The former corresponds to an internal magnetic-field energy of

$$U_M^{in} = \frac{\mu_0 l}{32\pi} I_0^2 \cos^2 \omega t. \quad (\text{B1})$$

The external magnetic-field energy is difficult to determine accurately. As can be seen from Fig. 1(b), the magnetic field is mainly concentrated near the nanorod. Thus, as an approximation, we make a simple cutoff by considering the magnetic energy in a cylindrical region that has a length l , an inner radius r_0 , and an outer radius l (the outer radius is chosen in terms of the distribution length of the conduction current). The external magnetic energy is thus calculated as

$$U_M^{out} = \frac{\mu_0 l}{8\pi} (\ln 2\kappa) I_0^2 \cos^2 \omega t. \quad (\text{B2})$$

With the Eqs. (B1) and (B2), the total magnetic-field energy within and outside the nanorod becomes

$$U_M = \frac{\mu_0 l}{8\pi} (\ln 2\kappa + \frac{1}{4}) I_0^2 \cos^2 \omega t. \quad (\text{B3})$$

Therefore, by setting $U_M = (1/2)L_F I_m^2$, the Faraday inductance of the nanorod can be obtained as

$$L_F = \frac{\mu_0 l}{4\pi} (\ln 2\kappa + \frac{1}{4}). \quad (\text{B4})$$

Appendix C

The accumulation of free charges on the side and ends of the nanorod induces an enhanced electric field near the nanorod [see Fig. 1(c)]. For the two semispherical ends, the electric field excited outside (in the upper or lower space) can be obtained with the Gauss theorem as

$$E_r^{end} = \frac{i\rho_0 r_0^2}{\epsilon_0 \epsilon_d r^2} e^{-i\omega t}. \quad (\text{C1})$$

Consequently, the electric-field energy stored near the two semispherical ends becomes

$$U_E^{end} = \frac{2\pi r_0^3}{\epsilon_0 \epsilon_d} \rho_0^2 \sin^2 \omega t. \quad (\text{C2})$$

In the middle cylindrical region ($r \geq r_0$; $-0.5l + r_0 \leq z \leq 0.5l - r_0$), the electric field is governed by the surface charges distributed on the side of nanorod. Following the surface charge distribution [see Eq. (2)], one may suppose that the radial component of electric field has a similar format:

$$E_r^{side} = A_0 \sin(\pi z / l) e^{-i\omega t}, \quad (C3)$$

where A_0 is a coefficient to be determined. By using the Gauss theorem around the nanorod, the coefficient is written as $A_0 = i\rho_0 r_0 / \varepsilon_0 \varepsilon_d r$. Considering that the surface charge density and radial electric field grow from 0 to maximum when z increases from 0 to $\pm l/2$, we also make a cutoff in the calculation of electric-field energy (i.e., the range of r is chosen approximately from r_0 to $l/2$). Therefore, the electric-field energy associated with the free charges on the side of nanorod is

$$U_E^{side} = \frac{\pi r_0^3}{\varepsilon_0 \varepsilon_d} (\kappa - 2) (\ln \kappa) \rho_0^2 \sin^2 \omega t. \quad (C4)$$

Besides the above electric-field energy of the isolated free charges, there is an interaction between the positive and negative free charges on the nanorod, thus corresponding to a negative electric potential energy. This interaction energy can be counted simply by using the potential energy of a pair of positive and negative point charges ($\pm Q$) separated by a distance $\Delta z = 2l / \pi$, i.e., $U_E^p = -(\text{Re } Q)^2 / (4\pi \varepsilon_0 \varepsilon_d \Delta z)$.

With the use of Eq. (4), we obtain

$$U_E^p = -\frac{\kappa r_0^3}{\varepsilon_0 \varepsilon_d} \rho_0^2 \sin^2 \omega t. \quad (C5)$$

According to the above results [Eqs. (C2), (C4), and (C5)], the total electric energy stored in the plasmonic system can be calculated as

$$U_E = \frac{(2\pi - \kappa) + \pi(\kappa - 2) \ln \kappa}{8\varepsilon_0 \varepsilon_d \kappa l} Q_0^2 \sin^2 \omega t. \quad (C6)$$

By setting $U_E = Q_m^2 / 2C$ (where $Q_m = Q_0 \sin \omega t$), the capacitance is determined as

$$C = \frac{4\varepsilon_0 \varepsilon_d \kappa l}{(2\pi - \kappa) + \pi(\kappa - 2) \ln \kappa}. \quad (C7)$$

References

- [1] E. Ozbay, Plasmonics: Merging Photonics and Electronics at Nanoscale Dimensions. *Science* 311, 189 (2006).
- [2] C. Genet and T.W. Ebbesen, Light in tiny holes. *Nature* 445, 39 (2007).
- [3] W. Chen, H. Hu, W. Jiang, Y. Xu, S. Zhang, and H. Xu, Ultrasensitive nanosensors based on localized surface plasmon resonances: From theory to applications. *Chin. Phys. B* 27, 107403 (2018).
- [4] N. Felidj, J. Aubard, G. Levi, J. R. Krenn, A. Hohenau, G. Schider, A. Leitner, F. R. Aussenegg, Optimized Surface-Enhanced Raman Scattering on Gold Nanoparticle Arrays. *Appl. Phys. Lett.* 82, 3095 (2003).
- [5] R. Antoine, P. F. Brevet, H. H. Girault, D. Bethell, D. J. Schiffrin, Surface Plasmon Enhanced Non-Linear Optical Response of Gold Nanoparticles at the Air/Toluene Interface. *Chem. Commun.* 19, 1901 (1997).
- [6] D. J. de Aberasturi, A. B. Serrano-Montes, and L. M. Liz-Marzán, Modern Applications of Plasmonic Nanoparticles: From Energy to Health. *Adv. Opt. Mater.* 3, 602 (2015).
- [7] P. Zijlstra, J. W. M. Chon, M. Gu, Five-dimensional optical recording mediated by surface plasmons in gold nanorods. *Nature* 459, 410 (2009).
- [8] L. A. Sweatlock, S. A. Maier, and H. A. Atwater, J. J. Penninkhof, A. Polman, Highly confined electromagnetic fields in arrays of strongly coupled Ag nanoparticles. *Phys. Rev. B* 71, 235408 (2005).
- [9] C. P. Huang, X. G. Yin, L. B. Kong, and Y. Y. Zhu, Interactions of nanorod particles in the strong coupling regime. *J. Phys. Chem. C* 114, 21123 (2010).
- [10] T. Kosako, Y. Kadoya, H. F. Hofmann, Directional control of light by a nano-optical Yagi-Uda antenna, *Nat. Photonics* 4, 312 (2010).
- [11] N. Yu, P. Genevet, M. A. Kats, F. Aieta, J.P. Tetienne, F. Capasso, Z. Gaburro, Light Propagation with Phase Discontinuities: Generalized Laws of Reflection and Refraction. *Science* 334, 333 (2011).
- [12] F. Qin, L. Ding, L. Zhang, F. Monticone, C. C. Chum, J. Deng, S. Mei, Y. Li, J. Teng, M. Hong, S. Zhang, A. Alù, C.W. Qiu, Hybrid bilayer plasmonic metasurface efficiently manipulates visible light. *Sci. Adv.* 2, e1501168 (2016).
- [13] J. Zhang, M. ElKabbash, R. Wei, S. C. Singh, B. Lam and C. Guo, Plasmonic metasurfaces with 42.3% transmission efficiency in the visible. *Light: Science &*

Applications 8, 53 (2019).

- [14] C.P. Huang, X.G. Yin, Q.J. Wang, H. Huang, and Y.Y. Zhu, Long-wavelength optical properties of a plasmonic crystal. *Phys. Rev. Lett.* 104, 016402 (2010).
- [15] D. J. Park, C. Zhang, J. C. Ku, Y. Zhou, G. C. Schatz, C. A. Mirkin, Plasmonic photonic crystals realized through DNA-programmable assembly. *Proceedings of the National Academy of Sciences of the United States of America* 112, 977 (2015).
- [16] N. S. Mueller, Y. Okamura, B. G. M. Vieira, S. Juergensen, H. Lange, E. B. Barros, F. Schulz, S. Reich, Deep strong light-matter coupling in plasmonic nanoparticle crystals. *Nature* 583, 780 (2020).
- [17] C. F. Bohren and D. R. Huffman, *Absorption and Scattering of Light by Small Particles* (Wiley, New York, 1983).
- [18] Y.Y. Yu, S.S. Chang, C.L. Lee, and C. R. C. Wang, Gold Nanorods: Electrochemical Synthesis and Optical Properties. *J. Phys. Chem. B* 101, 6661 (1997).
- [19] S. Link, M. B. Mohamed, and M. A. El-Sayed, Simulation of the Optical Absorption Spectra of Gold Nanorods as a Function of Their Aspect Ratio and the Effect of the Medium Dielectric Constant. *J. Phys. Chem. B* 103, 3073 (1999).
- [20] E. S. Kooij and B. Poelsema, Shape and size effects in the optical properties of metallic nanorods. *Phys. Chem. Chem. Phys.* 8, 3349 (2006).
- [21] H. Kuwata, H. Tamaru, K. Esumi, K. Miyano, Resonant light scattering from metal nanoparticles: Practical analysis beyond Rayleigh approximation, *Appl. Phys. Lett.* 83, 4625 (2003).
- [22] S. W. Prescott and P. Mulvaney, Gold nanorod extinction spectra. *J. Appl. Phys.* 99, 123504 (2006).
- [23] L. Novotny, Effective Wavelength Scaling for Optical Antennas. *Phys. Rev. Lett.* 98, 266802 (2007).
- [24] C.P. Huang, X.G. Yin, H. Huang, and Y.Y. Zhu, Study of plasmon resonance in a gold nanorod with an LC circuit model. *Opt. Express* 17, 6407 (2009).
- [25] E. Yablonovitch suggested using a more suitable model rather than the two-disk one to calculate the capacitance of nanorod (private communication, 2010).
- [26] N. Engheta, A. Salandrino, and A. Alu, Circuit Elements at Optical Frequencies: Nanoinductors, Nanocapacitors, and Nanoresistors. *Phys. Rev. Lett.* 95, 095504 (2005).

- [27] D. Zhu, M. Bosman, and J.K. W. Yang, A circuit model for plasmonic resonators. *Opt. Express* 22, 9809 (2014).
- [28] D. M. Sullivan, *Electromagnetic Simulation Using the FDTD Method* (IEEE, New Jersey, 2000).
- [29] M. Liu, P. Guyot-Sionnest, T.W. Lee, S. K. Gray, Optical properties of rodlike and bipyramidal gold nanoparticles from three-dimensional computations. *Phys. Rev. B* 76, 235428 (2007).
- [30] J.A. Schuller, E.S. Barnard, W. Cai, Y. C. Jun, J.S. White, M. I. Brongersma, Plasmonics for extreme light concentration and manipulation. *Nat. Mater.* 9, 193 (2010).